J|A|C|S

A R T I C L E S

Investigation of Zr−C, Zr−N, and Potential Agostic Interactions in an Organozirconium Complex by Experimental Electron Density Analysis

Sebastien Pillet,[†,§] Guang Wu,[†] Vichien Kulsomphob,[‡] Benjamin G. Harvey,[‡] Richard D. Ernst,*,[‡] and Philip Coppens*,[†]

Contribution from the Department of Chemistry, University of New York at Buffalo, Buffalo, New York 14260, and Department of Chemistry, University of Utah, Salt Lake City, Utah 84112

Received August 30, 2002 ; E-mail: ernst@chemistry.chem.utah.edu, coppens@acsu.buffalo.edu

Abstract: The crystal structure and electron density (ED) distribution of an imine coupling product with an open zirconocene, Zr(2,4-C₇H₁₁)[(*i*-Pr)NCHPhCH₂CMe=CHCMe=CH₂] (C₇H₁₁ = dimethylpentadienyl), have been derived from accurate synchrotron X-ray diffraction measurements. The molecular structure reveals asymmetric coordination of Zr by the pentadienyl (2,4-C₇H₁₁) ligand (⟨Zr−C⟩ = 2.56(6) Å), the butadiene fragment (⟨Zr−C⟩ = 2.43(5) Å), and the amide nitrogen atom (Zr−N = 2.0312(5) Å) of the second ligand. The study of the ED and its topological analysis affords new insight into the bonding and electronic structure of the title zirconium complex. The interactions between the metal center and the ligands are represented by a Zr−N bond path and one Zr−C bond path with each of the pentadienyl and butadiene moieties, contrary to the usually depicted global metal−ligand bonding. The butadiene and pentadienyl groups exhibit a polarization of the corresponding π-like ED in the C−Zr directions, indicating that the whole conjugated systems are nonetheless involved. The 4d atomic orbitals of Zr exhibit unusual populations according to ligand field considerations, which reveal a high degree of σ-donation from the conjugated π systems of both ligands. As deduced from numerical integration over the topologically defined atomic basins, the Zr to ligand charge transfer is 1.48 e to the C₁₇NH₂₄ ligand and 0.68 e to dimethylpentadienyl. Topological analysis of a short intramolecular Zr···(C,H) contact provides no indication of the presence of agostic interactions, despite a small Zr−N−C angle of 102.87(4)°. Thus, no bond path and BCP (bond critical point) of the ED are found in the Zr···(C,H) region, which would have provided evidence for such direct interactions, nor is there any evidence for charge accumulation between the Zr and H atoms, or for lengthening of the C−H bond involved in the putative interaction. These characteristics, similar to those in other distorted situations, may be common for other electron-deficient d⁰ complexes.

Introduction

Metal pentadienyl compounds have been found to display a great deal of diversity in their structural nature as well as a rich variety of reaction chemistry, including coupling reactions, naked metal chemistry, and applications in metal film depositions, syntheses of new materials, and catalysis.[1] Open and half-open titanocenes and zirconocenes have provided especially valuable insight in this regard, most notably by demonstrating that pentadienyl ligands may be both more strongly bound and more reactive than their cyclopentadienyl counterparts.[2−4] In

terms of chemistry, their coupling reactions with alkynes have proven to be particularly interesting, in several cases leading to complexes in which C−C single bonds have been constructed in bonding proximity to titanium,[1] and agostic interactions have been proposed on the basis of lengthened C−C bonds, dramatically reduced ¹³C−¹³C coupling constants, and supporting theoretical studies.[5]

In a related reaction of an open zirconocene with an imine, a Zr−N−C−H group has been generated with the unusually small Zr−N−C angle of 102.87(4)°, as compared to a value of 130.4(4)° in a similar titanium complex.[6] Although a (C−H)···Zr interaction was first suspected, the observation of a rather normal C−H coupling constant, ca. 125 Hz, did not provide support for this. However, the observation in another complex that a Ti interaction with a C−C bond could occur even in the presence of a C−H bond,[1] together with the fact that other complexes are known in which a metal center interacts

† University of New York at Buffalo.
‡ University of Utah.
§ Present address: Laboratoire de Cristallographie et Modélisation des Matériaux Minéraux et Biologiques, LCM3B, UMR 7036, UHP Nancy I, 54506 Vandoeuvre les Nancy cedex, France.

(1) Ernst, R. D. *Comments Inorg. Chem*. **1999**, *21*, 285−325.
(2) Hyla-Kryspin, I.; Waldman, T. E.; Melendez, E.; Trakarnpruk, W.; Arif, A. M.; Ziegler, M. L.; Ernst, R. D.; Gleiter, R. *Organometallics* **1995**, *14*, 5030−5040.
(3) Wilson, A. M.; West, F. G.; Rheingold, A. L.; Ernst, R. D. *Inorg. Chim. Acta* **2000**, *300−302*, 65−72.
(4) Kulsomphob, V.; Harvey, B. G.; Arif, A. M.; Ernst, R. D. *Inorg. Chim. Acta* **2002**, *334*, 17−24.
(5) Tomaszewski, R.; Hyla-Kryspin, I.; Mayne, C. L.; Arif, A. M.; Gleiter, R.; Ernst, R. D. *J. Am. Chem. Soc.* **1998**, *120*, 2959−2960.
(6) Tomaszewski, R.; Lam, K.-C.; Rheingold, A. L.; Ernst, R. D. *Organometallics* **1999**, *18*, 4174−4182.

preferentially with a Si−C bond rather than with a C−H bond,[7,8] raised the possibility of a (C−N)···Zr interaction in the imine coupling product, perhaps in conjunction with a (C−H)···Zr interaction. As the nature of the bonding in various agostic and σ-bond complexes is directly and fundamentally related to the oxidative addition process,[9,10] and therefore also to many other types of important bond activation reactions[11] and to processes of major technical significance (e.g., olefin polymerizations[12−17]), an understanding of the interactions which characterize such species is clearly desirable.

Experimental and theoretical electron density (ED) analysis has become an attractive tool to investigate the bonding and electronic structure of metal-based compounds.[18,19] Insight into the nature of metal−ligand interactions and metal−metal bonding has been obtained, especially in the framework of the "quantum theory of atoms in molecules" (QTAIM).[20] The physical and chemical applications range from purely organometallic systems[21] to intermetallic[22] and metallic clusters.[23,24] Such studies have been mostly restricted to first-row transition metal complexes, as anharmonic thermal motion at all but the lowest experimental temperatures complicates the analysis of heavier transition metal complexes. The use of synchrotron radiation allows measurements on very small crystal samples at short wavelengths, thus drastically decreasing sources of uncertainty such as absorption or extinction.[25] As shown here, the study of heavier-atom containing systems is now a realistic possibility.

Metallocenes have already been the subject of several ED studies. A topological analysis of the ED of group 2 metallocenes has been reported by Bytheway et al.[26] from Hartree−Fock (HF) and density functional theory (DFT) methods. Bader et al.[27,28] introduced and used the concept of localization and delocalization indexes to investigate bonding between Ti and cyclopentadienyl, diene, and alkyl fragments.[5] Antipin et al.[29] have analyzed the experimental ED of vanadocene, and, more generally, the nature of interactions in π-ligands η^2 coordinated to a metal atom has been investigated in a series of studies by Macchi et al.[30,31]

The goals of the study presented here are to probe the electronic nature of the interactions between zirconium and several key classes of ligands and to investigate the origin of the short intramolecular Zr···H and Zr···C contacts present in the title complex, which may represent an agostic interaction, in analogy with those found in a number of other Zr complexes.[32,33] The concepts of the charge density analysis, applied here and in previous studies (see, for example, Scherer et al.[34]), allow the characterization of the nature of such interactions. To our knowledge, this work represents the first ED study and topological analysis of a zirconium complex, as well as the first experimental examination of metal coordination involving diene, open dienyl, and amide ligands.

This paper is divided into four parts. Following this introduction, the Experimental Details section describes the X-ray diffraction measurements and the data reduction and charge density refinement. The crystal structure and ED results are discussed in the Results section, with a focus on the metal−ligand interactions and the putative agostic Zr···H bond. Concluding remarks are given in the final section.

Experimental Details and Electron Density Refinement

Synthesis and Spectroscopic Characterization. All synthetic and spectroscopic procedures were carried out under a nitrogen atmosphere in Schlenk apparatus or in a glovebox. $Zr(2,4-C_7H_{11})_2(PMe_3)$ was prepared by a published procedure,[35] while organic reagents were purchased commercially. Solvents were dried and degassed by distillation from sodium/benzophenone under a nitrogen atmosphere. Spectroscopic studies were carried out as previously described.[36]

$Zr(2,4-C_7H_{11})[(i-Pr)NCHPhCH_2CMe=CHCMe=CH_2]$. To a magnetically stirred solution of 0.60 g (1.7 mmol) of $Zr(2,4-C_7H_{11})_2(PMe_3)$ $(C_7H_{11} =$ dimethylpentadienyl) in 50 mL of THF under nitrogen at −78 °C was added 0.50 mL (3.4 mmol) of *N*-benzylidene isopropylamine. The initial green solution was allowed to warm to room temperature and was stirred for 4 h. A gradual color change from dark green to dark red was observed. The solvent was removed in vacuo, and the crude product was extracted with three 20 mL portions of pentane. The extracts were filtered through a Celite pad on a coarse frit and concentrated to ca. 15 mL. The solution was placed into a −30 °C freezer overnight, yielding large, dark red cubic crystals (0.33 g, 45% yield, mp 91−94 °C). This compound is very air- and moisture-sensitive, but it can be stored under nitrogen indefinitely without apparent decomposition. Occasionally, the sample can be contaminated by a small amount of starting material which is easily removed by fractional crystallization. Smaller crystals, more suitable for the electron density analysis, were obtained by cooling a concentrated solution in

(7) Klooster, W. T.; Brammer, L.; Schaverien, C. J.; Budzelaar, P. H. M. *J. Am. Chem. Soc.* **1999**, *121*, 1381−1382.
(8) Koga, N.; Morokuma, K. *J. Am. Chem. Soc.* **1988**, *110*, 108−112.
(9) Kubas, G. J.; Unkefer, C. J.; Swanson, B. I.; Fukushima, E. *J. Am. Chem. Soc.* **1986**, *108*, 7000−7009.
(10) Kubas, G. J. *Metal Dihydrogen and σ-Bond Complexes*; Kluwer Academic/ Plenum: New York, 2001.
(11) Stahl, S. S.; Labinger, J. A.; Bercaw, J. E. *Inorg. Chem.* **1998**, *37*, 2422−2431.
(12) Yang, X.; Stern, C. L.; Marks, T. J. *J. Am. Chem. Soc.* **1994**, *116*, 10015−10031.
(13) Resconi, L.; Piemontesi, F.; Franciscono, G.; Abis, L.; Fiorani, T. *J. Am. Chem. Soc.* **1992**, *114*, 1025−1032.
(14) Eshuis, J. J. W.; Tan, Y. Y.; Meetsma, A.; Teuben, J. H.; Renkema, J.; Evens, G. G. *Organometallics* **1992**, *11*, 362−369.
(15) Schmidt, G. F.; Brookhart, M. *J. Am. Chem. Soc.* **1985**, *107*, 1443−1444.
(16) Ivin, K. J.; Rooney, J. J.; Stewart, C. D.; Green, M. L. H.; Mahtab, R. *J. Chem. Soc., Chem. Commun.* **1978**, 604−606.
(17) Turner, H. W.; Schrock, R. R.; Fellmann, J. D.; Holmes, S. J. *J. Am. Chem. Soc.* **1983**, *105*, 4942−4950.
(18) Coppens, P. *X-ray Charge Densities and Chemical Bonding*; Oxford University Press: New York, 1997.
(19) Koritsanszki, T. S.; Coppens, P. *Chem. Rev.* **2001**, *101*, 1583−1628.
(20) Bader, R. F. W. *Atoms in Molecules: A Quantum Theory*; Clarendon Press: New York, 1990.
(21) Pillet, S.; Souhassou, M.; Mathoniere, C.; Lecomte, C., to be published.
(22) Gavoille, G.; Hansen, N. K.; Welter, R.; Malaman, B.; Krane, H. G.; Herzig, P. *J. Phys.: Condens. Matter* **2000**, *12*, 2667−2679.
(23) Macchi, P.; Proserpio, D. M.; Sironi, A. *J. Am. Chem. Soc.* **1998**, *120*, 13429−13435.
(24) Macchi, P.; Garlaschelli, L.; Martinengo, S.; Sironi, A. *J. Am. Chem. Soc.* **1999**, *121*, 10428−10429.
(25) Coppens, P.; Wu, G.; Volkov, A.; Abramov, Y.; Zhang, Y.; Fullagar, W. K.; Ribaud, L. *Trans. Am. Crystallogr. Assoc.* **1999**, *34*, 51−64.
(26) Bytheway, I.; Popelier, P. L. A.; Gillespie, R. J. *Can. J. Chem.* **1996**, *74*, 1059−1071.
(27) Fradera, X.; Austen, M. A.; Bader, R. F. W. *J. Phys. Chem. A* **1999**, *103*, 304−314.
(28) Bader, R. F. W.; Matta, C. F. *Inorg. Chem.* **2001**, *40*, 5603−5611.

(29) Antipin, M. Y.; Lyssenko, K. A.; Boese, R. *J. Org. Chem.* **1996**, *61*, 259−262.
(30) Macchi, P.; Proserpio, D. M.; Sironi, A. *J. Am. Chem. Soc.* **1998**, *120*, 1447−1455.
(31) Macchi, P.; Schultz, A. J.; Larsen, F. K.; Iversen, B. B. *J. Phys. Chem. A* **2001**, *105*, 9231−9242.
(32) Meier, R. J.; van Doremaele, G. H. J.; Iarlori, S.; Buda, F. *J. Am. Chem. Soc.* **1994**, *116*, 7274−7281.
(33) Woo, T. K.; Fan, L.; Ziegler, T. *Organometallics* **1994**, *13*, 2252−2261.
(34) Scherer, W.; Hieringer, W.; Spiegler, M.; Sirsch, P.; McGrady, G. S.; Downs, A. J.; Haaland, A.; Pedersen, B. *Chem. Commun.* **1998**, 2471−2472.
(35) Waldman, T. E.; Stahl, L.; Wilson, D. R.; Arif, A. M.; Hutchinson, J. P.; Ernst, R. D. *Organometallics* **1993**, *12*, 1543−1552.
(36) Newbound, T. D.; Stahl, L.; Ziegler, M. L.; Ernst, R. D. *Organometallics* **1990**, *9*, 2962−2972.

Table 1. Crystallographic Data and Experimental Details (T_{min} and T_{max} are the Minimum and Maximum Transmission Coefficients)

$a/b/c$ (Å)	8.5981(4)/9.3991(5)/27.0670(9)
β (deg)/V (Å³)/Z	97.482(4)/2168.8(2)/4
space group/crystal system	$P2_1/n$/monoclinic
temperature (K)/wavelength (Å)	16/0.6361
scan method	ω
frame width (deg)	0.3
exposure time per frame (s)	7 (at $2\theta = 27°$)/10 (at $2\theta = 65°$)
no.measured/ independent reflections	43 676/13 948
range of $h/k/l$	$-20 < h < 19, 0 < k < 20,$ $0 < l < 43$
R_{int} (I) (%)	2.78
$(\sin\theta/\lambda)$ max (Å⁻¹)	1.17
mean redundancy	3.0
μ (mm⁻¹)/T_{min}/T_{max}	2.16/0.85/0.87

pentane to -60 °C overnight. All NMR assignments were corroborated utilizing HETCOR 2D NMR techniques.

¹H NMR (benzene-d_6, ambient): δ 7.1–7.4 (m, 5H, phenyl), 4.97 (s, 1H), 4.91 (s, 1H), 4.51 (d, 1H, C(H)(C$_6$H$_5$), $J = 6.5$ Hz), 3.90 (s, 1H), 3.26 (s, 1H), 2.90 (dd, 1H), 2.45 (septet, 1H, C(H)(CH$_3$)$_2$, $J = 6.6$ Hz), 2.41 (d, 1H, $J = 6.5$ Hz), 2.20 (dd, 1H, $J = 6.0, 1.0$ Hz), 2.17 (s, 1H), 2.16 (s, 3H, CH$_3$), 2.09 (s, 3H, CH$_3$), 1.85 (s, 3H, CH$_3$), 1.61 (d, 1H, $J = 2.5$ Hz), 1.52 (s, 3H, CH$_3$), 1.42 (s, 2H), 0.81 (2d, 6H, CH$_3$ on NC(H)(CH$_3$)$_2$, $J = 6.0$ Hz).

¹³C NMR (benzene-d_6, ambient): δ 150.0 (s, 1C on phenyl), 137.7 (s, 1C), 136.3 (s, 1C), 126–130 (m, 5C, phenyl), 118.9 (s), 116.7 (d, 1C, $J = 153$ Hz), 91.8 (d, 1C, $J = 163$ Hz), 83.4 (s, 1C), 81.2 (t, 1C, $J = 157$ Hz), 80.7 (t, 1C, $J = 157$ Hz), 72.4 (d, (C$_6$H$_5$)CH, $J = 131$ Hz), 52.0 (t, 1C, $J = 150$ Hz), 46.1 (d, CH(CH$_3$)$_2$, $J = 128$ Hz), 45.3 (t, 1C, $J = 128$ Hz), 32.4, 30.3, 29.4, 28.4, 25.2, 22.5 (6q, 6CH$_3$, $J =$ ca. 125 Hz).

Anal. Calcd for C$_{24}$H$_{35}$NZr: C, 67.23; H, 8.23; N, 3.26. Found: C, 67.07; H, 8.12; N, 3.08.

Data Collection and Reduction. An irregularly shaped single crystal of dimensions $0.11 \times 0.10 \times 0.06$ mm³ was mounted on a Huber four-cycle diffractometer at the SUNY X3A1 beamline at the National Synchrotron Light Source at Brookhaven National Laboratory. The sample was cooled to ∼16 K using an open helium gas-flow system.[37] Data were collected by the φ-scan method (frame width $\Delta\varphi = 0.3°$) using two different detector settings. Low angle data were measured at a detector position of $2\theta = 27°$, using a 7 s per frame exposure time (33 483 reflections on 1800 frames). To ensure high-resolution, crucial for an accurate charge density study, 502 frames (10 193 reflections) were measured using a detector position of $2\theta = 65°$ and 10 s exposure time. The data were corrected for oblique incidence of the reflected beams on the phosphor of the SMART6000 CCD detector.[38]

For heavy atom containing crystals, the data accuracy can be strongly affected by absorption effects, which have been very much reduced in the present experiment by the small sample size. Because the crystal faces could not be unambiguously indexed, an empirical absorption correction was performed assuming a mean spherical crystal of 0.05 mm radius ($\mu = 2.16$ mm⁻¹) and fitting the transmission surface using SORTAV.[39] The resulting minimum and maximum transmission coefficients are $T_{min} = 0.85$ and $T_{max} = 0.87$. Next 43 676 reflections were reduced and merged in Laue group $2/m$ to give 13 948 unique reflections up to a resolution of $S = \sin\theta/\lambda = 1.17$ Å⁻¹. The low internal agreement indices ($R_{int} = 2.78\%$ (2.81% before absorption correction) and $R_w = 3.20\%$, redundancy = 3.0) support the good quality and consistency of the merged data set. Crystallographic and data collection details are reported in Table 1.

(37) Ribaud, L.; Wu, G.; Zhang, Y.; Coppens, P. *J. Appl. Crystallogr.* **2001**, *34*, 76–79.
(38) Wu, G.; Rodrigues, B.; Coppens, P. *J. Appl. Crystallogr.* **2002**, *35*, 356–359.
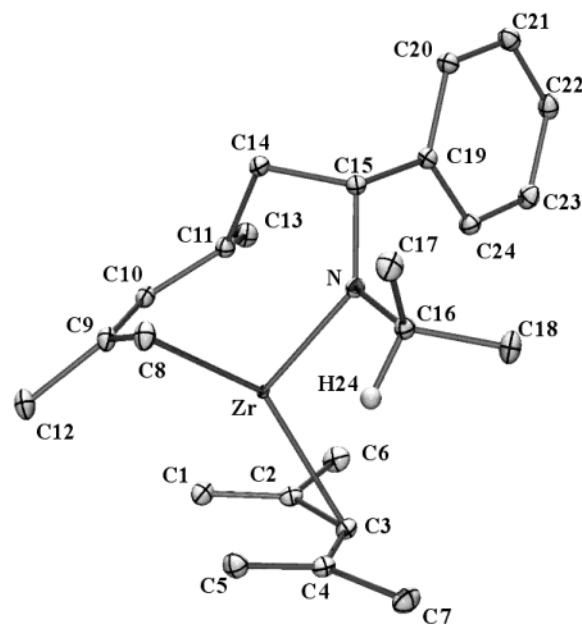(39) Blessing, R. H. *J. Appl. Crystallogr.* **1989**, *22*, 396–397.

Figure 1. ORTEP view and atom numbering scheme of Zr(2,4-C$_7$H$_{11}$)(NMe$_2$-CHPhCH$_2$CMe=CHCMe=CH$_2$). Ellipsoids drawn at the 50% level probability and arbitrary radius for H24. H atoms (except H24) omitted for clarity.

Structure and Charge Density Refinements. To get a starting molecular geometry for the subsequent ED fitting, the crystal structure was solved in the $P2_1/n$ space group by direct methods and refined by full matrix least-squares on F^2 using SHELX.[40] Non-hydrogen atoms were refined anisotropically using all reflections ($I > 0$). Hydrogen atoms were located in Fourier difference maps and refined isotropically ($R = 3.32\%$, $R_w = 5.94\%$, and GOF = 0.757). ORTEP views of the molecular structure and the crystal packing are presented in Figures 1 and 2, while a detailed analysis of the crystal structure is given in the next section. This independent atom model is referred to below as model I.

In a following refinement, the ED was fitted using the multipole model,[41] according to the Hansen and Coppens formalism as implemented in the MOLLY program.[42] In this model, the ED is described as a superposition of nonspherical pseudoatoms (eq 1):

$$\rho(\vec{r}) = \rho_{core}(r) + P_v\kappa^3\rho_{val}(\kappa r) + \sum_{l=0}^{l_{max}}\kappa'^3 R_{in}(\kappa' r)\sum_{m=0}^{+l}P_{lm}\pm d_{lm}\pm(\theta,\varphi) \tag{1}$$

where $\rho_{core}(r)$ and $\rho_{val}(r)$ correspond, respectively, to spherically averaged Hartree–Fock core and valence electron densities for isolated atoms. κ and κ' are contraction–expansion parameters, and P_v is the electron population of the corresponding atomic valence shell. Real spherical harmonics ($d_{lm}\pm$) describe the anisotropy of the valence ED through the multipole population parameters $P_{lm}\pm$. The atomic core ED $\rho_{core}(r)$ was fixed during the ED fitting, assuming no perturbation due to chemical bonding.

For the N, C, and H atoms, the core and valence atomic spherical electron densities were calculated from Clementi Hartree–Fock wave functions for ground-state isolated atoms.[43] The following coefficients [($n_l = 2, 2, 3$, $\zeta_l = 3.00$ Bohr⁻¹) for N, ($n_l = 2, 2, 3$, $\zeta_l = 3.14$ Bohr⁻¹) for C, and ($n_l = 2$, $\zeta_l = 2.26$ Bohr⁻¹) for H] were used for the Slater-type radial functions $R_{in}(r) = (\xi^{n_l+3}/(n_l + 2)!)r^{n_l}e^{-\xi_{l'}r}$. The multipolar expansion was limited to the orders $l_{max} = 3$ (octupole) for N and C,

(40) Sheldrick, G. M. *SHELXL93*; University of Göttingen: Germany, 1993.
(41) Stewart, R. F. *J. Chem. Phys.* **1973**, *58*, 1668–1676.
(42) Hansen, N. K.; Coppens, P. *Acta Crystallogr., Sect. A* **1978**, *34*, 909–921.
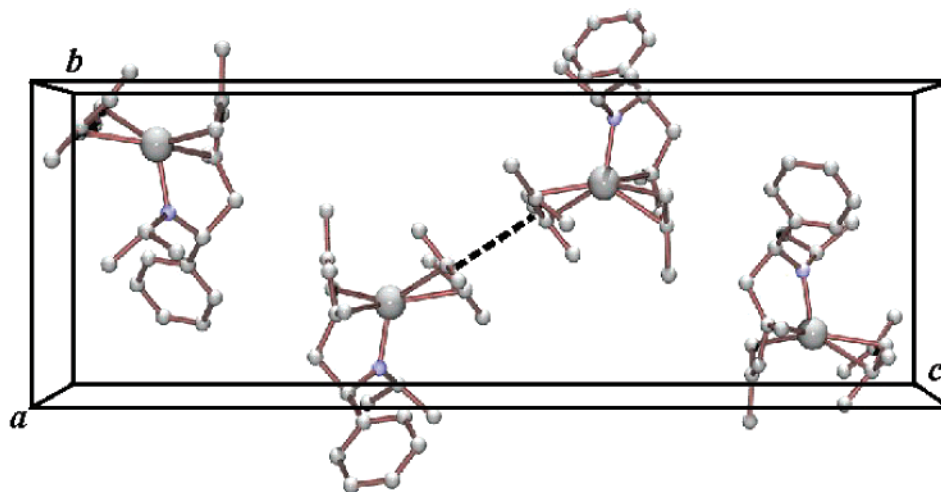(43) Clementi, E.; Roetti, C. *At. Data Nucl. Data Tables* **1974**, *14*, 177–478.

Figure 2. Crystal packing. $\pi-\pi$ intermolecular contacts between dimethylpentadienyl anions are depicted as dashed lines.

and $l_{max} = 1$ (dipole) for H. The anomalous dispersion coefficients were taken from Kissel et al.,[44] as computed from relativistic Hartree–Fock Slater wave functions. Only one (κ, κ') set was used for the H atoms, with κ' for the dipolar functions fixed at unity. Chemical constraints were also applied to the other κ and κ' parameters, including three different constraints for the C atoms (one each for the phenyl C atoms, the sp^2, and sp^3 C atoms). Extinction effects were not significant.

In molecular complexes such as the zirconocenes, the Zr atom can adopt valence states varying from 0 to IV. Therefore, different starting hypotheses of the electron configuration corresponding to neutral zirconium ((Kr)5s^{2}4d^2), the Zr^{2+} ion ((Kr)4d^2 and (Kr)5s^2), and the Zr^{4+} ion were tested, even though a 2+ or 4+ formal charge is expected for the present complex, depending on whether the diene ligand is formally neutral or dianionic (enediyl). For each model, Zr core and spherical valence atomic scattering factors were derived from relativistic wave functions of Zr, as tabulated by Macchi and Coppens.[45] The radial scattering factors of the 4d and 5s electrons of zirconium differ less than the corresponding 3d and 4s scattering of the first row transition metal elements, preventing a clear distinction between the spherical components of the two shells. Because of the high correlation between the corresponding population parameters, one monopole was assigned to the 5s electrons, and one monopole was assigned to the 4d electrons without refining both simultaneously. In the following, the starting configurations (Kr)5s^{2}4d^2 and (Kr)4d^2 correspond to models III and IV, respectively. In model III, the monopole population corresponding to the 5s electrons was kept fixed at 2 electrons, whereas the population of the monopole describing the spherical 4d shell was varied during the refinement procedure. In model IV, the monopole population corresponding to the 5s electrons was fixed at zero, and the second monopole population corresponding to the 4d electrons was fitted. The multipole expansion was limited to the order $l_{max} = 4$ (hexadecapole) with the following radial exponents ($n_l = 6, 6, 6, 6, \zeta_l = 6.00$).

The starting atomic positions were taken from the SHELX refinement, and the C–H bond lengths were normalized to the usual neutron values (1.08 Å)[46] by shifting the hydrogen atoms along the C–H directions. The positions and thermal parameters for non-hydrogen atoms were first refined against the high angle data ($S > 0.8$ Å^{-1}) to deconvolute thermal smearing effects and ED. The valence ED was then fitted against low angle data ($S < 0.8$ Å^{-1}) in successive cycles on P_v, κ, $P_{lm}\pm$, and κ' parameters, while constraining the electroneutrality of the crystal, until convergence was reached. In the final cycles,

Table 2. Atomic Positions (Fractional Coordinates) and U_{eq} ($U_{eq} = (U_{11} + U_{22} + U_{33})/3$ in Å^2) Values

atom	x	y	z	U_{eq}
Zr	0.990868(6)	0.193780(6)	0.127798(2)	0.00688(2)
N	0.96722(6)	0.40568(5)	0.13947(2)	0.0102(2)
C1	0.85918(8)	−0.03849(7)	0.08687(2)	0.0125(2)
C2	0.84358(7)	0.07307(7)	0.05278(2)	0.0103(2)
C3	0.97093(7)	0.15434(7)	0.03692(2)	0.0103(2)
C4	1.13688(7)	0.14226(7)	0.05147(2)	0.0105(2)
C5	1.21119(7)	0.06045(7)	0.09074(2)	0.0128(2)
C6	0.67939(8)	0.12219(8)	0.03233(2)	0.0150(3)
C7	1.23901(8)	0.24569(8)	0.02678(2)	0.0151(2)
C8	1.14064(7)	0.15113(7)	0.20552(2)	0.0114(2)
C9	1.00907(7)	0.05419(7)	0.20341(2)	0.0102(2)
C10	0.84788(7)	0.09247(7)	0.19262(2)	0.0100(2)
C11	0.77430(7)	0.22687(6)	0.17984(2)	0.0101(2)
C12	1.04715(8)	−0.10369(7)	0.20690(2)	0.0141(3)
C13	0.59968(8)	0.21761(7)	0.16101(2)	0.0141(3)
C14	0.82266(8)	0.36622(7)	0.20732(2)	0.0111(2)
C15	0.87564(7)	0.48301(6)	0.17231(2)	0.0095(2)
C16	1.11223(7)	0.46495(6)	0.12439(2)	0.0098(2)
C17	1.22476(8)	0.52955(7)	0.16714(2)	0.0138(3)
C18	1.08358(8)	0.56714(8)	0.07984(2)	0.0151(3)
C19	0.73966(7)	0.57105(7)	0.14584(2)	0.0099(2)
C20	0.67061(7)	0.67635(7)	0.17304(2)	0.0115(2)
C21	0.54780(8)	0.76106(7)	0.15034(2)	0.0131(3)
C22	0.49034(8)	0.74073(7)	0.10002(2)	0.0133(3)
C23	0.55660(8)	0.63463(7)	0.07288(2)	0.0134(3)
C24	0.68081(8)	0.55108(7)	0.09565(2)	0.0121(2)

both charge density and conventional (positional and thermal) parameters were refined.

Chemical constraints were applied to the hydrogen atom valence ED (identical P_v and $P_{lm}\pm$ parameters); these constraints were relaxed at the end of refinement. Tables 2 and 3 summarize atomic positions and selected bond lengths and angles at the end of multipolar refinement (model III). The Hirshfeld rigid bond test[47] indicates that a reasonable deconvolution between ED and thermal smearing effects was achieved. The mean difference between the mean-square displacements of two bonded atoms along the bond is 0.0011 Å^2 for C–C and C–N bonds. The Zr–C and Zr–N bonds present a higher mean difference (0.0040 Å^2), as expected for nonsimilar weight atoms.

The agreement factors are summarized in Table 4. The different refinements agree on the essential features of the electron distribution. In the following, we will only discuss the results of model III, which we believe to be the most reliable. The residual density for model III is shown in Figure 3. The low residual density attests to the quality of the modeled ED.

(44) Kissel, L.; Zhou, B.; Roy, S. C.; Sen Gupta, S. K.; Pratt, R. H. *Acta Crystallogr., Sect. A* **1995**, *51*, 271–288 (http://www-phys.llnl.gov/Research/scattering/index.html).

(45) Macchi, P.; Coppens, P. *Acta Crystallogr., Sect. A* **2001**, *57*, 656–662.

(46) Allen, F. H. *Acta Crystallogr., Sect. B* **1986**, *42*, 515–522.

(47) Hirshfeld, F. L. *Acta Crystallogr., Sect. A* **1976**, *32*, 239–244.
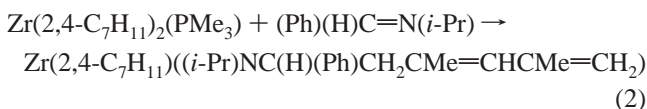
Table 3. Selected Bond Lengths (Å) and Angles (deg)

Bond Lengths			
Zr−C1	2.6359(6)	Zr−C8	2.3535(6)
Zr−C2	2.5189(6)	Zr−C9	2.4190(6)
Zr−C3	2.4714(6)	Zr−C10	2.4613(6)
Zr−C4	2.5988(6)	Zr−C11	2.4963(6)
Zr−C5	2.5808(7)	Zr−N	2.0309(5)
Zr···H24	2.4604(6)		
C1−C2	1.3918(9)	C4−C5	1.3971(9)
C2−C3	1.4454(9)	C2−C6	1.5195(9)
C3−C4	1.4344(9)	C4−C7	1.5217(9)
C8−C9	1.4479(8)	C10−C11	1.4347(8)
C9−C10	1.4248(9)	C11−C13	1.5239(9)
C9−C12	1.5199(9)	C11−C14	1.5366(9)
N−C15	1.4564(8)	N−C16	1.4710(8)
C1···C3^a	3.9777(8)	C2···C5^a	4.0509(8)
C1···C4^a	3.8741(8)	C3···C3^a	3.595(1)
C2···C3^a	3.7436(9)	C3···C4^a	3.7119(8)
C2···C4^a	3.4944(8)	C3···C5^a	4.1301(8)

Bond Angles			
C1−C2−C3	125.71(6)	C3−C4−C5	126.33(6)
C2−C3−C4	129.91(6)	C1−C2−C6	118.37(6)
C5−C4−C7	116.92(5)	C8−C9−C10	125.68(6)
C9−C10−C11	131.18(6)	C8−C9−C12	116.81(6)
C14−C11−C13	113.78(5)		

^{a} $2 - x, -y, -z$.

Table 4. Agreement Factors for the Different Refinement Models

| model	N_{par}	R (%)	R_w (%)	GOF
I (SHELX)	375	3.37	6.04	0.77
II (spherical)	441	3.15	2.33	1.12
III (multipolar)	1211	2.71	1.58	0.76
IV (multipolar)	1211	2.77	1.64	0.79

Results

Synthesis and Characterization. The reaction of $Zr(2,4-C_7H_{11})_2(PMe_3)$ with 1 equiv of *N*-benzylidene isopropylamine leads to a selective 1:1 coupling reaction (eq 2). The somewhat

$$Zr(2,4-C_7H_{11})_2(PMe_3) + (Ph)(H)C=N(i\text{-}Pr) \rightarrow$$
$$Zr(2,4-C_7H_{11})((i\text{-}Pr)NC(H)(Ph)CH_2CMe=CHCMe=CH_2) \quad (2)$$

air-sensitive product was readily isolated as a crystalline solid and fully characterized through analytical and spectroscopic data. These data were fully consistent with the expected formulation of such a species (**1**). In particular, the complexities of the ^1H and ^{13}C NMR spectra were consistent with the lack of any symmetry, and one of the four CH_2 groups displayed a low $J(^{13}C-H)$ value, 128 Hz versus 150−157 Hz for the other three, indicative of the former's expected sp^3 hybridization brought about by its coupling to the imine carbon atom.[48] On the basis of the above data, then, complex **1** was expected to possess η^5-dienyl, η^4-diene, and π-amide coordination, leading straightforwardly to its formulation as a 16-electron complex, analogous to related titanium complexes.[6,49]

Molecular Structure. The unit cell consists of four symmetry-related zirconium complexes, $Zr(2,4-C_7H_{11})(C_{17}NH_{24})$ $(C_{17}NH_{24} = [(i\text{-}Pr)NCHPhCH_2CMe=CHCMe=CH_2], C_7H_{11} =$ dimethylpentadienyl). This complex represents a case of a bent (i.e., nonparallel olefinic ligands) M(dienyl)(diene)(L) com-

1
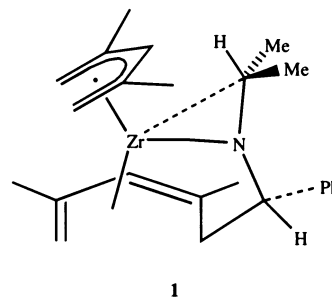
plex,[36,50] in which the zirconium center is coordinated by a dimethylpentadienyl ligand and by the butadiene fragment of the $C_{17}NH_{24}$ ligand (Figure 1). The coordination sphere of Zr is at least formally completed by the N atom of the $C_{17}NH_{24}$ ligand with a Zr−N distance of 2.0312(5) Å. The Zr−C distances range from 2.3531(6) to 2.6358(6) Å with a mean value of 2.50(8) Å, in line with those reported for other Zr-$(2,4-C_7H_{11})_2$ compounds,[35] $Zr(2,4-C_7H_{11})_2(PEt_3)$ ($\langle Zr-C \rangle$ = 2.49(3) Å), $Zr(2,4-C_7H_{11})_2(CO)$ ($\langle Zr-C \rangle$ = 2.45(2) Å), $Zr(2,4-C_7H_{11})_2(CO)_2$ ($\langle Zr-C \rangle$ = 2.52(3) Å), $Zr(C_5H_7)_2(dmpe)$ ($\langle Zr-C \rangle$ = 2.49(3) Å).[51]

The mean distance to the Zr atom is longer for the $2,4-C_7H_{11}$ ligand (2.56(6) Å) than for the butadiene moiety of the second ligand (2.43(5) Å), the zirconium atom thus being displaced toward the butadiene. A difference in terms of bond strength is therefore expected and confirmed by the following ED analysis. The short Zr−N contact causes the butadiene and pentadienyl ligands to be nonparallel, with an angle of 33.49(4)° between the corresponding best planes.

The pentadienyl group is almost planar, with a root-mean-square deviation from the best plane of 0.04 Å, the C6 and C7 atoms being displaced from the plane by 0.241(1) and 0.066(1) Å, respectively. The central C2−C3 and C3−C4 bond lengths differ from the C1−C2 and C4−C5 bond lengths by 0.045(3) Å, revealing a difference in bond orders in the conjugated system as, for example, in $Zr(2,4-C_7H_{11})_2(CO)_2$ and $Zr(2,4-C_7H_{11})_2$-(CO),[35] which arises from a contribution from resonance structure **2**. Similarly, the butadiene fragment of the $C_{17}NH_{24}$

2
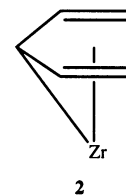
ligand exhibits an almost perfect planarity with a root-mean-square deviation from the best plane of only 0.01 Å, C12 and C13 being out of the plane by 0.228(1) and 0.256(1) Å, respectively. The C−C bond lengths in the butadiene fragment (1.4479(8), 1.4248(9), and 1.4347(8) Å for C8−C9, C9−C10, and C10−C11, respectively) do not exhibit single/double bond alternation. This is consistent with significant contributions from both η^4-diene (**3**) and η^4-enediyl (**4**) resonance forms, the latter of which would be expected to lead to shorter Zr−C distances

(48) Yasuda, H.; Tatsumi, K.; Nakamura, A. *Acc. Chem. Res.* **1985**, *18*, 120−126.
(49) Tomaszewski, R.; Arif, A. M.; Ernst, R. D. *J. Chem. Soc., Dalton Trans.* **1999**, 1883−1890.
(50) Newbound, T. D.; Arif, A. M.; Wilson, D. R.; Rheingold, A. L.; Ernst, R. D. *J. Organomet. Chem.* **1992**, *435*, 73−84.
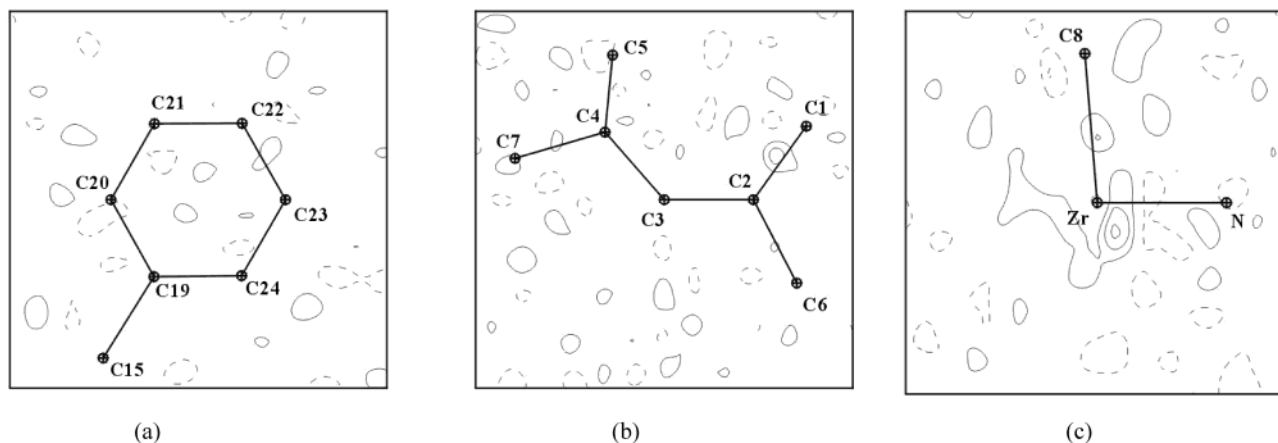(51) Waldman, T. E.; Rheingold, A. L.; Ernst, R. D. *J. Organomet. Chem.* **1995**, *503*, 29−33.

Figure 3. Residual density in (a) the phenyl ring, (b) the pentadienyl ligand, and (c) the Zr−N−C8 plane ($S < 0.8$ Å^{-1}). Contours of 0.1 e Å^{-3}, positive as solid lines and negative as dashed lines.

for the terminal carbon atoms.[52,53] The location of the zirconium center below the diene plane is inconsistent, however, with an η^2-enediyl (**5**) contribution.[54]
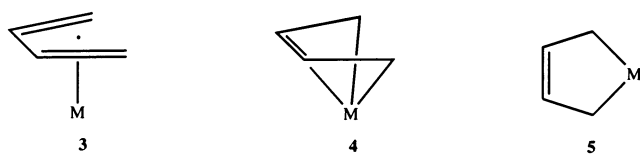
The intramolecular Zr···H24 contact of 2.4604(6) Å may represent an agostic interaction. The small Zr−N−C16 angle (102.86(4)°), as compared to 130.4(4)° for the Ti−N−C angle in a similar titanium complex,[6] indicates a distortion of the C15−N−C16 moiety. However, the 2.4604(6) Å distance is longer than some other reported Zr···H agostic bonds (2.14 Å in $(SiH_2Cp_2)ZrC_3H_7^+$, 2.20 Å in $Cp_2ZrCH_3^+$)[32] involved in the catalytic action of zirconocenes in the polymerization of olefins,[32,33] although longer distances have been observed, such as 2.48 Å $Zr(CH_2SiMe_3)_4(dmpe)$.[55] Furthermore, the N−C16 and C16−H24 bonds (the latter before extension to the neutron value) are not significantly lengthened, contrary to what would be expected on the basis of an agostic Zr···H24 interaction.[32,33] However, this may not be necessary for an agostic interaction, given that H_2 "σ complexes" are known in which the H−H distance is similar to that in free H_2.[56] More criteria are therefore needed and will be provided from the detailed analysis of the ED.

As shown in Figure 2, the dimethylpentadienyl ligands of two neighboring complexes stack in parallel with short C−C distances between the two center-of-symmetry related dimethylpentadienyl ligands (Table 3). The contacts involve π−π and (C−H)−π interactions,[57] as confirmed by the following electron density analysis.

Molecular Graph and Binding Modes. According to the AIM theory, a direct interatomic interaction is unambiguously indicated by the existence of a bond path (line of maximum of

ED), linking the two bonded atoms and characterized by the topological properties at the corresponding bond critical point (BCP, minimum of ED along the bond path).

The molecular graph ("union of the closures of the bond paths"[20]) deduced from the topological analysis of the experimental density with the NEWPROP program[58] is shown in Figure 4. As expected, bond paths and BCPs are associated with all C−C, C−N, and C−H bonds. For the symmetric configuration of a metal bonded to an aromatic ring, bond paths link the metal center to each of the aromatic C atoms, as calculated by Bytheway et al.[26] for group 2 metallocenes (M = Mg or Ca), although Bader and Matta[28] observed either three or four bond paths (at RHF and DFT levels, respectively) linking Ti with a cyclopentadienyl ligand in another complex. In the present case, in addition to the strong Zr−N interaction, only two Zr−C contacts exhibit a bond path, one for each of the dimethylpentadienyl (to C3) and dimethylbutadiene (to C8) moieties.

The positive sign of the Laplacian of the ED at both the Zr−C8 and the Zr−C3 BCPs is as observed generally for metal ligand interactions.[19] Although according to the AIM theory a positive value of the Laplacian at the BCP characterizes a closed-shell interaction, different concepts have been developed in recent work. In addition to ρ_{BCP} and $\nabla^2\rho_{BCP}$, the local kinetic and total energy densities at the BCPs, $G(\rho_{BCP})$ and $E(\rho_{BCP})$, respectively, which can be derived from the electron density using a functional proposed by Abramov,[59] have been used in a density-based characterization of metal−metal and metal−ligand bonding,[24] leading to a different classification of bond types.

One bond path, following a straight line, links the outside carbon atom C8 of the butadiene fragment to Zr. No direct bonding to the interior carbon atoms C9 and C10 or to C11 is evident from the molecular graph. A related enediyl bonding scheme implying two bond paths has been found by Bader et al.[28] for Ti−butadiene interactions in a complex in which, as in the current compound, the butadiene bonds do not show bond length alternation.

(52) Yasuda, H.; Nakamura, A. *Angew. Chem., Intl. Ed. Engl.* **1987**, *26*, 723−742.
(53) Erker, G.; Krüger, C.; Müller, G. *Adv. Organomet. Chem.* **1985**, *24*, 1−39.
(54) Murakami, M.; Itami, K.; Ito, Y. *Organometallics* **1999**, *18*, 1326−1336.
(55) Cayias, J. Z.; Babaian, E. A.; Hrncir, D. C.; Bott, S. G.; Atwood, J. L. *J. Chem. Soc., Dalton Trans.* **1986**, 2743−2744.
(56) Van Der Sluys, L.; Eckert, J.; Eisenstein, O.; Hall, J. H.; Huffman, J. C.; Jackson, S. A.; Koetzle, T. F.; Kubas, G. J.; Vergamini, P. J.; Caulton, K. G. *J. Am. Chem. Soc.* **1990**, *112*, 4831−4841.

(57) Hunter, C. A.; Sanders, J. K. M. *J. Am. Chem. Soc.* **1990**, *112*, 5525−5534.
(58) (a) Souhassou, M.; Blessing, R. H. *J. Appl. Crystallogr.* **1999**, *32*, 210−217. (b) Souhassou, M. "Atomic properties from electron densities: program Newprop-int", ECM XIX, Nancy 2000, abstract S2-M2-P2.
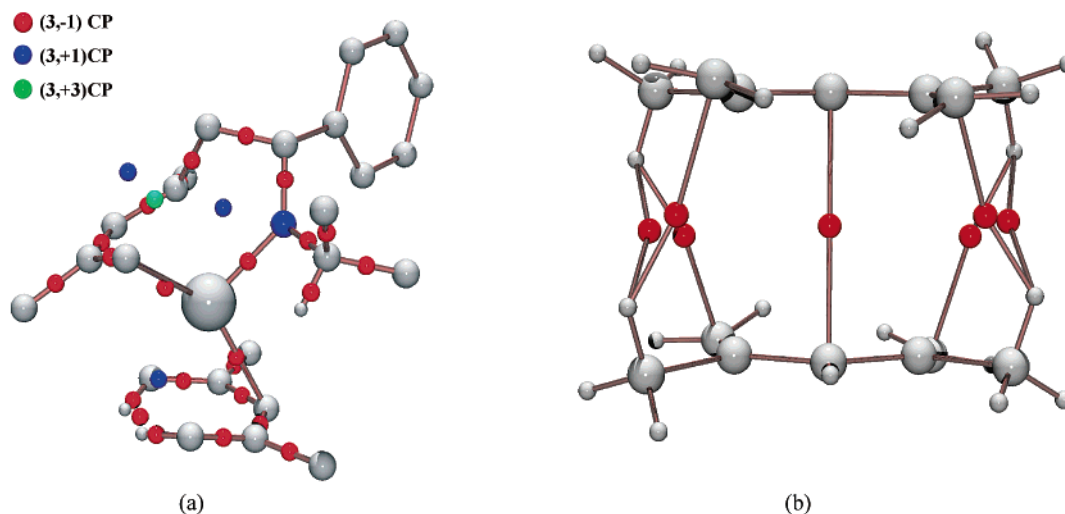(59) Abramov, Y. A. *Acta Crystallogr., Sect. A* **1997**, *53*, 264−272.

Figure 4. Localization of the critical points of the electron density in (a) the Zr coordination sphere and (b) the interdimer region. Only relevant critical points are depicted.

The ED at the BCP is lower for Zr−C3 (0.31 e Å^{-3}) than for Zr−C8 (0.42 e Å^{-3}), in agreement with the asymmetry in the coordination distances and therefore the strengths of the interactions with the butadiene and pentadienyl groups. The strongest interaction occurs with the nitrogen atom, the ED at the Zr−N BCP being 0.88 e Å^{-3}.

The interactions in the present zirconium compound are certainly more extensive than the binding suggested by the experimental molecular graph. Given that complexes with substantial enediyl character typically exhibit pronounced long−short−long carbon−carbon bond patterns,[2,52−54,60] the absence of bond length alternation of the butadiene group suggests a similar contribution of the three C−C bonds in the coordination interactions, contrary to what the molecular graph indicates. Theoretical evidence on metal carbonyl clusters shows that bonding interactions can exist even in the absence of a bond path.[61] In addition, the Zr atom is positioned below the diene and dienyl ligands, in contrast to expectations based on **5** and **6**. For the dienyl coordination, the C3−Zr vector has rotated 70° from the expected location based on **6**. A closer analysis of the ED provides further insight into the nature of the bonding.

6
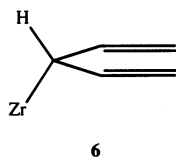
Electron Density around Zr and the 4d Atomic Orbital Populations. The deformation of the valence ED of zirconium is illustrated in Figure 5c,d, and a 3D representation is given in Figure 6. Two kidney-shape lobes of positive deformation density are directed toward the conjugated systems of both ligands (maximum of 0.6 e Å^{-3}), and four negative lobes (minimum of −0.5 e Å^{-3}) are located in the perpendicular plane. The local coordinate system for Zr has been chosen according to these directions, assuming that the z axis is along the positive lobes and the x axis is pointing toward the nitrogen atom. The

positive lobes correspond to an increase of the 4d$_{z^2}$ orbital population with regards to the isolated zirconium atom (the 5s^{2}4d^2 valence electronic state has been taken as reference), whereas the negative lobes indicate a depopulation of the 4d$_{xy}$ atomic orbital. The kidney shape of the positive lobes results from the enediyl coordination mode, which elongates the deformation density in the Zr−C8−C11 plane. The Zr 4d orbital populations, derived from the multipolar expansion of the deformation density,[62] are listed in Table 5. Using only the 4d monopole to derive the 4d atomic orbital populations leads to an inconsistent negative population for the 4d$_{xz}$ orbital, likely due to the impossibility of deconvoluting the 5s and 4d electrons into two separate monopoles, as discussed above. We have therefore adjusted the 4d orbital populations in Table 5 by shifting 5s electrons equally into all d orbitals, such that the population of the 4d$_{yz}$ orbital becomes equal to zero. Such an adjustment is clearly appropriate, given the fact that the 4d orbitals are substantially stabilized relative to the 5s orbital for either Zr^{2+} or Zr^{4+}. Table 5 shows good qualitative agreement between models III and IV after the 5s electron transfer.

The characteristics of the deformation density and 4d orbital populations can be understood in the context of the Dewar−Chatt−Duncanson model,[63,64] which has found support in numerous charge density studies. Both delocalized ligands donate π ED to the d$_{z^2}$ atomic orbital of zirconium through σ-bonding (Figure 6b), which implies that the occupied frontier molecular orbitals in this zirconium complex exhibit a high metal 4d$_{z^2}$ character. Similar π-donation interactions should involve the 4d$_{xz}$ orbital, which has a relatively large population (Table 5). More surprising are the low occupancy of the 4d$_{xy}$ orbital and a significant occupancy of the 4d$_{x^2−y^2}$ orbital, contrary to what is expected from usual crystal field arguments. In the *XY* plane (Figure 5c), the lone pair of nitrogen is spread out and directed toward Zr through σ-donation into the Zr 4d$_{x^2−y^2}$ atomic orbital (Figure 6c), evidenced by its electron occupancy. In addition to this N → Zr σ-donation, the nitrogen atom donates π electron density to Zr by N(2p)−Zr(4d$_{xz}$) orbital overlap,

(60) Arif, A. M.; Ernst, R. D.; Melendez, E.; Rheingold, A. L.; Waldman, T. E. *Organometallics* **1995**, *14*, 1761−1769.
(61) Macchi, P.; Sironi, A. *Coord. Chem. Rev.*, in press.
(62) Holladay, A.; Leung, P.; Coppens, P. *Acta Crystallogr., Sect. A* **1983**, *39*, 377−387.
(63) Dewar, M. J. S. *Bull. Soc. Chim. Fr.* **1951**, C71−C79.
(64) Chatt, J.; Duncanson, L. A. *J. Chem. Soc.* **1953**, 2939−2947.
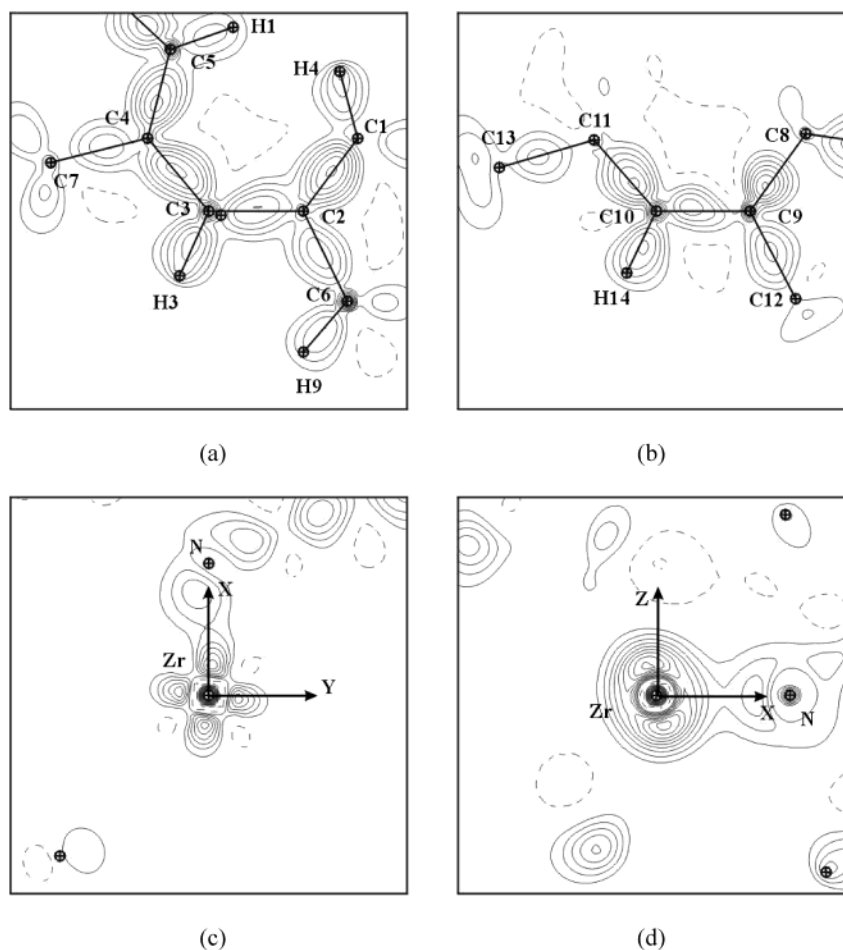
Figure 5. Static deformation density for model III in (a) the dimethylpentadienyl ligand, (b) the butadiene fragment, (c) the *xy* coordination plane of Zr, and (d) the *xz* coordination plane of Zr. In part d, the N atom is out of the plane. Contours are as in Figure 3.

consistent with the above-noted occupancy of the $4d_{xz}$ atomic orbital (Figure 6d). It is possible that the low occupancy of the $4d_{xy}$ orbital may derive from a δ back-bonding interaction, and, in fact, pentadienyl ligands have been proposed to serve generally as strong δ acids. The high formal metal oxidation state in this case would seem to preclude much of this, although it could be that such an interaction with the diene ligand contributes to its enediyl character. This issue will need to be addressed through additional studies.

The QTAIM provides a unique decomposition of the electron density of the system in open subsystems (the atomic basins), delimited by interatomic surfaces, defined according to the zero flux condition in the gradient vector field of the electron density as $\nabla\rho\cdot\vec{n} = 0$. The atomic and fragment charges from numerical integration over the atomic basins,[65] derived using program NEWPROP,[58] are given in Table 6. The results indicate a charge transfer of 2.16 e from the Zr atom to the ligands, more localized on the $C_{17}NH_{24}$ ligand (1.48 e) than on dimethylpentadienyl (0.68 e). The N atom has a considerable charge of -1.05 e, indicating high electrostatic Zr−N interactions in addition to the $\sigma-\pi$ N → Zr donations discussed above. Bader et al.[28] report a high charge transfer of "approximately 3 e" from Ti to cyclopentadienyl and diene fragments in a similar complex.

Electron Density Distribution of the Dimethylpentadienyl Ligand. In addition to the BCPs located in each of the covalent C−C and C−H bonds, an H···H bond path formally closes the

open edge of the dimethylpentadienyl ligand. This feature is of interest given the observation that metal pentadienyl complexes can undergo loss of H_2 under thermal conditions or during mass spectroscopic studies, with conversion to cyclopentadienyl.[66−68] A related bond path is not found for the diene ligand, which is characterized by a longer open edge.

The static deformation density (total ED minus ED for isolated atoms) in the plane of the dimethylpentadienyl ligand is shown in Figure 5a. The features in the C1−C2, C2−C3, C3−C4, and C4−C5 bonds are similar, as expected from electronic conjugation effects. The ED and Laplacians at the BCPs in the C−C bonds mirror the differences in bond lengths (Table 7). The ellipticities of the C−C bonds of the dimethyl-pentadienyl ligand show the same pattern. The ellipticity averages 0.12 for the longer C4−C7 and C2−C6 bonds, 0.22 for C2−C3 and C3−C4, and 0.25 for the shorter C1−C2 and C4−C5 bonds. The differences in bond lengths, ED at the BCP, and ellipticity consistently reflect the distortion of the penta-dienyl conjugated system as a result of the interactions with

(65) Pillet, S.; Souhassou, M.; Lecomte, C.; Rabu, P.; Massobrio, C.; Drillon, M. *Phys. Rev. B*, submitted.
(66) Mann, B. E.; Manning, P. W.; Spencer, C. M. *J. Organomet. Chem.* **1986**, *312*, C64−C66.
(67) Kralik, M. S.; Rheingold, A. L.; Ernst, R. D. *Organometalics* **1987**, *6*, 2612−2614.
(68) Kirss, R. U.; Quazi, A.; Lake, C. H.; Churchill, M. R. *Organometalics* **1993**, *12*, 4145−4150.
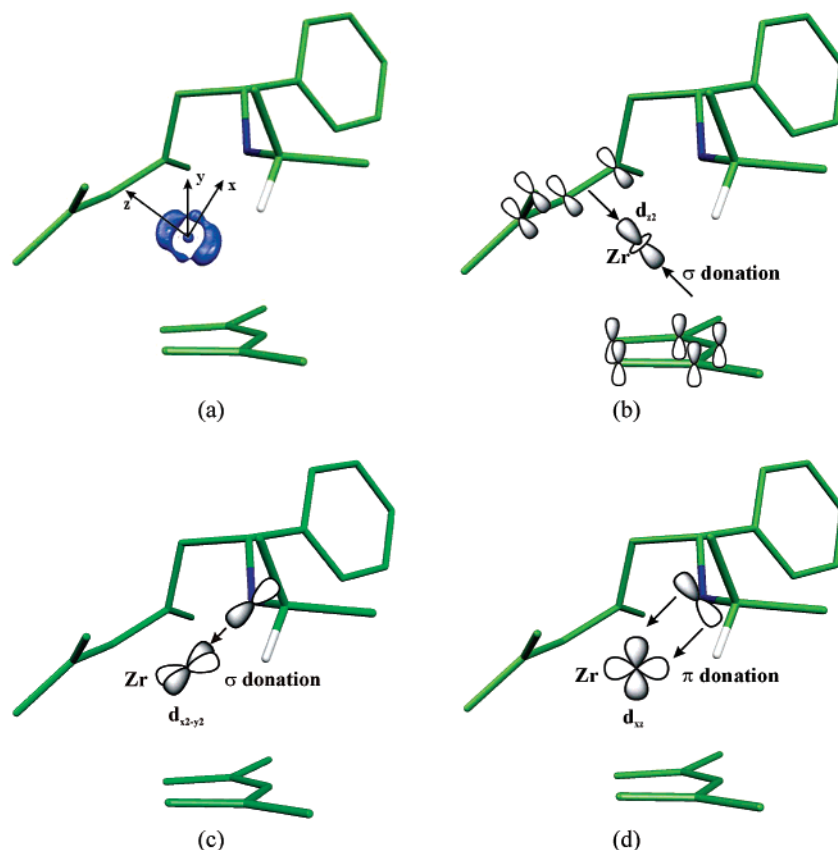
Figure 6. Three-dimensional representation of (a) the static deformation density around Zr atom for model III and schematic representation of the (b) Zr ← diene σ donation, (c) Zr ← N σ donation, and (d) Zr ← N π donation. Isocontour of 0.2 e Å^{-3} (positive in blue).

Table 5. 4d Orbital Populations for the Zr Atom (in e)

model	$d_{x^2-y^2}$	d_{z^2}	d_{xy}	d_{xz}	d_{yz}	total
III (multipolar)	0.17(3)	0.43(3)	−0.24(3)	0.40(3)	−0.29(3)	0.47(7)
III (multipolar)^a	0.46(3)	0.72(3)	0.05(3)	0.69(3)	0.00(3)	1.92(7)
IV (multipolar)	0.60(3)	0.77(3)	0.22(3)	0.76(3)	0.11(3)	2.46(7)

^{a} After transferring 5s electrons to the 4d shell to eliminate the d_{xy} negative population (see text).

Table 6. Selected Atomic Charges from Numerical Integration over the Atomic Basins^a

atom	charge	atom	charge
Zr	+2.16	C8	−0.26
N	−1.05	C9	−0.23
C1	−0.46	C10	−0.36
C2	−0.12	C11	+0.00
C3	−0.44	C12	−0.23
C4	−0.08	C13	−0.35
C5	−0.26	H24	+0.06
C6	−0.41	$\langle H \rangle$	+0.13
C7	−0.46	C$_7$H$_{11}$ ligand	−0.68
		C$_{17}$NH$_{24}$ ligand	−1.48

^{a} The total charge obtained on the asymmetric unit is +0.011 e, whereas the integrated volume is 540.138 Å^3, which represent global errors of 0.004 and 0.4% due to the integration procedure.

Zr, the double-bond character being more localized on C1−C2 and C4−C5 (cf. **2**).

Figure 7 presents the deformation density in the planes bisecting the C−C bonds of the conjugated system. The ellipticity and therefore the π character of each are revealed by the elongation of the deformation density in the direction roughly perpendicular to the best plane. However, especially for the

Table 7. Topological Properties of the Electron Density at the BCPs^a

bond	d_1	d_2	d	$\rho(\vec{r}_{CP})$	$\nabla^2\rho(\vec{r}_{CP})$	ϵ
C11−C13	0.738	0.787	1.5239(9)	1.48	−8.4	0.14
C11−C10	0.660	0.775	1.4347(8)	1.89	−14.1	0.44
C10−C9	0.757	0.668	1.4248(9)	1.75	−11.1	0.65
C9−C8	0.860	0.589	1.4479(9)	1.67	−6.8	0.39
C9−C12	0.776	0.744	1.5199(9)	1.60	−10.3	0.08
C11−C14	0.766	0.770	1.5366(9)	1.57	−9.6	0.10
C1−C2	0.657	0.736	1.3918(9)	2.01	−14.7	0.26
C2−C3	0.735	0.711	1.4454(9)	1.93	−14.0	0.26
C3−C4	0.719	0.717	1.4344(9)	1.85	−12.5	0.18
C4−C5	0.682	0.715	1.3971(9)	2.16	−18.4	0.25
C2−C6	0.788	0.732	1.5195(9)	1.51	−8.3	0.11
C4−C7	0.776	0.747	1.5217(9)	1.60	−9.95	0.14
N−C16	0.788	0.685	1.4710(8)	1.77	−7.82	0.01
Zr−N	1.071	0.960	2.0309(5)	0.86	7.7	
Zr−C3	1.255	1.219	2.4714(6)	0.31	3.5	
Zr−C8	1.155	1.212	2.3535(6)	0.42	4.2	
C3···C3^b	1.797	1.797	3.595(1)	0.03	0.3	
C1···H10^b	1.686	1.213	2.8077(6)	0.04	0.5	
C5···H7^b	1.850	1.287	3.0629(6)	0.02	0.3	
H10···H7^b	1.327	1.447	3.338(1)	0.03	0.4	

^{a} d is the bond length (Å); d_1 and d_2 are the distances (Å) from the CP to each of the linked atoms, respectively. $\rho(\vec{r}_{CP})$ and $\nabla^2\rho(\vec{r}_{CP})$ are the electron density (e Å^{-3}) and Laplacian (e Å^{-5}) of the electron density at the CP, respectively. ϵ is the dimensionless ellipticity of the bonds. ^{b} 2 − x, −y, −z.

C2−C3 bond, the principal axes of the ellipsoids deviate from this direction by a tilt toward the Zr atom. The π-like molecular orbitals are apparently not constructed from pure p$_z$ carbon orbitals (z perpendicular to the plane of the conjugated system), but they contain a significant contribution from the p$_x$ and p$_y$ orbitals. This observation provides experimental substantiation
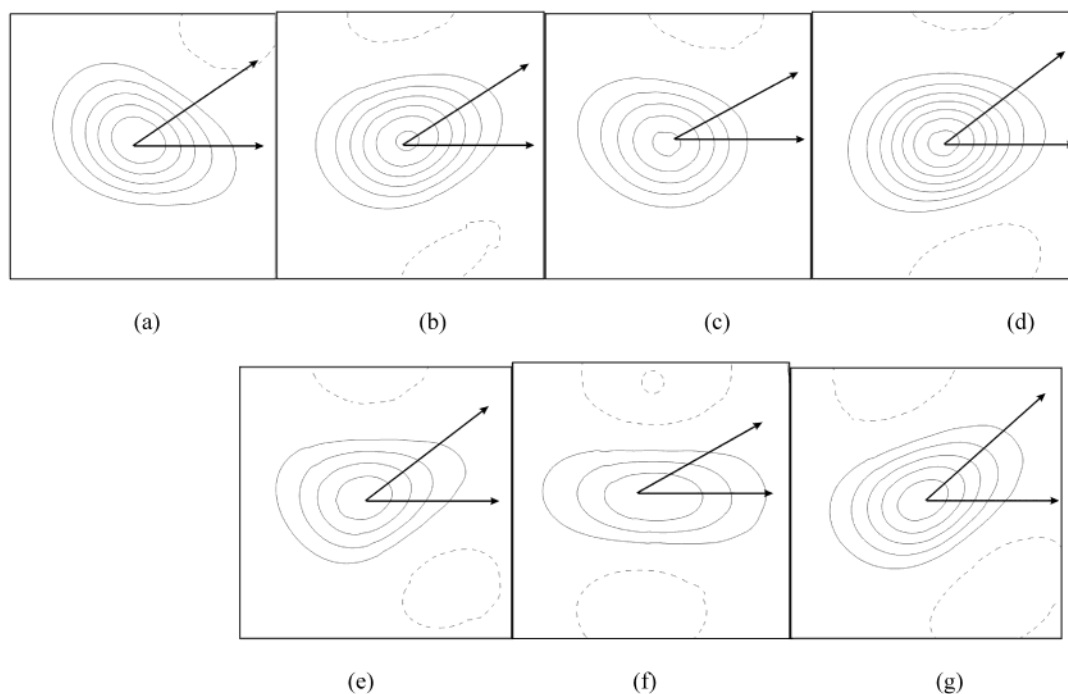
Figure 7. Deformation density in the plane bisecting to the (a) C1−C2, (b) C2−C3, (c) C3−C4, (d) C4−C5, (e) C8−C9, (f) C9−C10, and (g) C10−C11 bonds. The horizontal arrow represents the direction perpendicular to the best planes (pentadiene and butadiene), whereas the diagonal arrow represents the direction of the projection of Zr on the plane of the figure. Contours are as in Figure 3.

for the decades-old proposals, based upon observations of substituent tilts out of a given ligand plane, that the p orbitals of both cyclopentadienyl[69,70] and pentadienyl ligands[71] were in effect tilting (more accurately, rehybridizing) to optimize overlap with the more compact metal centers (e.g., **7**).

7
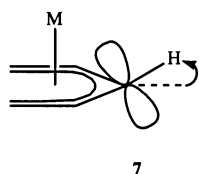
Thus, one again sees that the whole conjugated system of the pentadienyl ligand appears affected by the proximity of the transition metal atom.

Bader et al.[28] and Bytheway et al.[26] used the presence or absence of VSCCs (valence shell charge concentrations corresponding to maxima in the negative of the Laplacian) near the C atoms to detect and characterize bonding with Ti and Mg, respectively. A VSCC is located near C3 in the direction of Zr (Figure 8), but it is absent on C1, C2, C4, and C5, in accordance with the strong Zr−C3 interaction evident from the bond path analysis.

A three-dimensional representation of the total ED, illustrating the coordination of Zr by the pentadienyl group, is presented in Figure 9. The largest overlap between the atomic EDs occurs between Zr and C3. In addition, significant contacts between Zr and all of the C−C bonds are revealed, even though no bond paths are involved. The orientation of the π-like molecular

orbitals is evident from the shape of the surface, as indicated by the arrows in Figure 9.

As discussed previously, the zirconium complexes form dimers in which the dimethylpentadienyl ligands of two neighboring complexes stack parallel to each other. This particular geometry results from $\pi-\pi$[57] and (C−H)−π[72] intermolecular interactions, as indicated by the presence of a number of BCPs between the ligands (Figure 4b). As shown by the low ED at the corresponding BCPs (0.02−0.04 e Å^{-3}), the intermolecular interactions represented by these bond paths are nevertheless rather weak.

Electron Density Distribution of the Diene Fragment. The high ellipticities of the C8−C9, C9−C10, and C10−C11 bonds (0.39, 0.65, 0.44) mean that the corresponding ED is more elongated in the direction almost perpendicular to the plane of the conjugation (Figure 7). As for two of the bonds of the pentadienyl group, a tilt of the deformation density ellipsoids of the C8−C9 and C10−C11 bonds toward the Zr direction is observed. Therefore, even though an η^1 binding mode is implied by the molecular graph, the extended conjugated system interacts with the Zr atom. Because of the bending of the butadiene and pentadienyl fragments and the resulting differences in Zr−C bond lengths, the local distribution of BCP, RCP, and CCPs is also far less regular than that found for group 2 metallocenes.[26]

As in the pentadienyl ligand, the positions of the VSCC of the carbon atoms of the butadiene group (Figure 8) give evidence for localized Zr−C interactions, only C8 and C11 exhibiting VSCCs in the direction of the Zr atom, in accord with substantial enediyl character (i.e., **4**).

Potential Agostic Interactions. The short Zr⋯H24 and Zr−C16 distances (2.4604(6) and 2.7601(6) Å, respectively),

(69) Elian, M.; Chen, M. M. L.; Mingos, D. M. P.; Hoffmann, R. *Inorg. Chem.* **1976**, *15*, 1148−1155.
(70) Haaland, A. *Acc. Chem. Res.* **1979**, *12*, 415−422.
(71) Ernst, R. D. *Struct. Bonding (Berlin)* **1984**, *57*, 1−53.

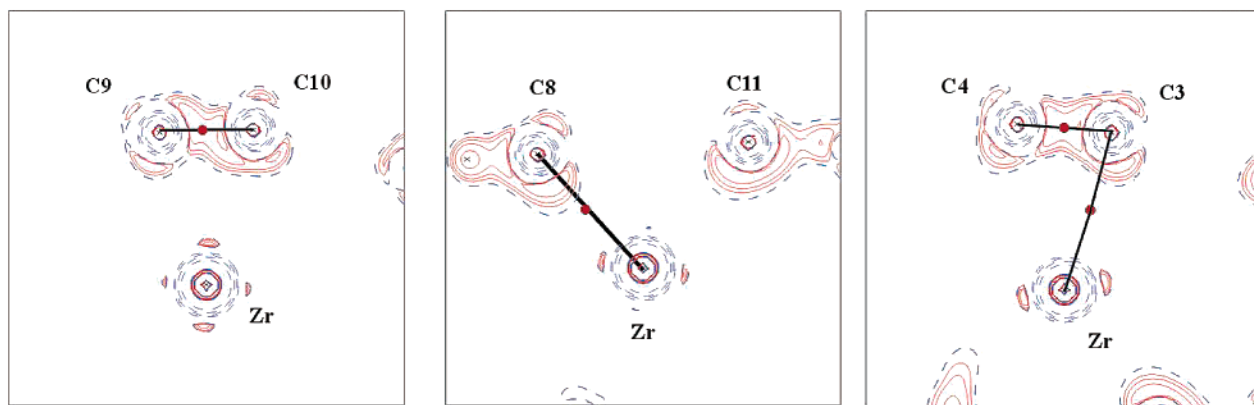(72) Nishio, M.; Hirota, M.; Umezawa, Y. *The CH−π Interaction*; Wiley-VCH: New York, 1998.

Figure 8. Contour map of the $L(_r^\rho) = -\nabla^2\rho(_r^\rho)$ function in the (a) Zr−C9−C10, (b) Zr−C8−C11, and (c) Zr−C4−C3 planes. Isocontours of $x \cdot 10^n$ e Å^{-5} with $n = 0, \pm1, 2$ and $x = 0, \pm2, \pm4, \pm8$, positive as red solid lines, negative as blue dashed lines. BCP and RCP are depicted as red and blue circles, respectively. Bond paths are represented by lines.
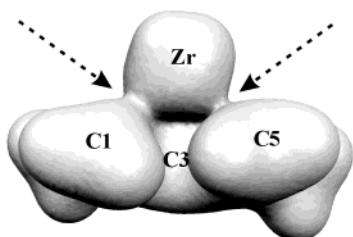

Figure 9. Three-dimensional representation of the electron density in the Zr-dimethylpentadienyl fragment. Isocontour of 0.2 e Å^{-3}. Dashed arrows show the contacts between Zr and the C1−C2 and C4−C5 bonds.

together with the small Zr−N−C16 angle of 102.86(4)°, suggest that an agostic interaction exists in the zirconium complex. Three-center (C−H)···M interactions are quite common[10,73−76] and would provide an explanation for the small Zr−N−C16 angle. Such complexes have been proposed to be in a state of arrested oxidative addition, leading to two general situations.[10,11] The first involves an early metal center with a d^0 configuration, so that oxidative addition cannot occur, and only a σ donor interaction from the C−H bond to the metal center exists. In other complexes, the presence of d electrons on the metal center allows for back-bonding into the C−H bond's σ^* orbital. In such cases, a stronger overall interaction is expected. While the present Zr complex appears to be an example of the former type, for which back-bonding should be precluded, the situation is more complicated in the specific case of β-agostic complexes. In a β-agostic ethyl complex, for example, the agostic interaction may still lead to transfer of the hydride to the d^0 metal center. In essence, as the formal C−H oxidative addition occurs, one can regard the complex as also undergoing a simultaneous C−C reductive elimination, converting the C−C bond to a C=C bond. In fact, for the present zirconium complex, then, the possibility of back-bonding to the C16−H24 bond does therefore exist, although there would be a replacement of the highly favorable Zr−N bonds (both σ and π) by the ensuing hydride and imine coordinations. The presence of the favorable Zr−N bond would therefore be expected to greatly inhibit the back-bonding
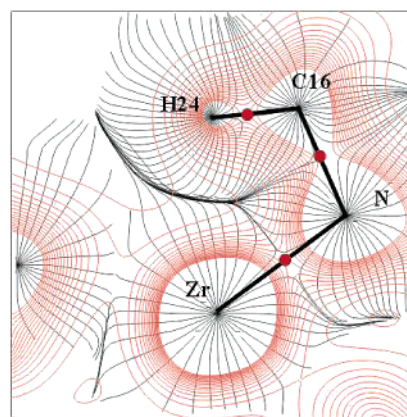
(73) Crabtree, R. H.; Holt, E. M.; Lavin, M.; Morehouse, S. M. *Inorg. Chem.* **1985**, *24*, 1986−1992.
(74) Crabtree, R. H. *Angew. Chem., Int. Ed. Engl.* **1993**, *32*, 789−805.
(75) Brookhart, M.; Green, M. L. H. *J. Organomet. Chem.* **1983**, *250*, 395−408.
(76) Brookhart, M.; Green, M. L. H.; Wong, L.-L. *Prog. Inorg. Chem.* **1988**, *36*, 1−124.

Figure 10. Gradient trajectories (black lines) and total electron density (red lines) for model III in the Zr−N−C16−H24 plane. Bond CPs are depicted as red circles. Contour levels of 0.1 e Å^{-3} are used for the total electron density. The gradient trajectories are computed in a slice and projected on the plane of the figure, so that some of them appear to cross each other.

component for the interaction. No BCP and bond path are found connecting Zr···H24 or Zr···C16 (Figure 10). There also is no apparent curvature in the Zr−N bond path, whereas at least in β-agostic alkyl complexes, bent M−C bond paths have been observed.[34] Conceivably, however, the high Zr−N bond strength might offset such a tendency. In a recent investigation of agostic bonding in an alkyllithium complex, Scherer et al. analyze the ellipticity of the C_α−Si bond in the Li−C_α−Si$_\beta$−C_γ−H$_\gamma$ backbone and conclude that delocalization rather than Li···H−C agostic interaction is responsible for the observed distortions of the molecule.[77] Such an explanation seems inapplicable to the current complex, as evidenced by the absence of ellipticity of the N−C16 bond. Finally, the atomic charge obtained by numerical integration over the atomic basin for H24 is positive (+0.05), as opposed to what had been observed by Popelier in a calculation on the α-agostic CH$_3$TiCl$_2$ cation;[78] this positive charge would be consistent with a primarily σ (donation) interaction.

As the ED results thus do not provide any indication for the existence of an agostic bridge in the zirconium complex, other

(77) Scherer, W.; Sirsch, P.; Shorokhov, D.; McGrady, G. S.; Mason, S. A.; Gardiner M. G. *Chem.-Eur. J.* **2002**, *8*, 2324−2334.
(78) Popelier, P. L. A.; Logothetis, G. *J. Organomet. Chem.* **1998**, *555*, 101−111.

physical evidence must be examined. There is first of all the small Zr−N−C angle, leading to a bend of ca. 27° toward the zirconium center, as compared to an analogous titanium complex. While one might attempt to attribute this tilt to a steric interaction, it does not seem reasonable that one species would tilt some 27° without the opposing species also undergoing a noticeable tilt, in the opposite direction. For complexes with a potential (C−H)···M interaction, Crabtree et al.[73] have defined the distance, d_{bp}, from the given metal center to the C−H bonding pair of electrons, and the effective covalent radius of the C−H bonding electrons r_{bp}, obtained by subtracting the metal radius from d_{bp}. From examination of these distances, they have "found no cases in which r_{bp} is less than 1.9 Å in an 18-electron complex," showing "that the C−H bond is not close to the metal simply by accident but that the 2-electron deficiency is *required* for bridging to occur."[73] In the present zirconium complex, d_{bp} is 2.51 Å, which, using a Zr radius of 1.60 Å, corresponds to an r_{bp} value of ∼0.9 Å. This is well below the 1.9 Å limit and thus indicative of a metal−C−H interaction. The M−H−C angle is calculated as 94.32(3)°, again in a typical range for accepted agostic interactions.

The lack of an apparent reduction in the C−H coupling constant appears to argue against a (C−H)···Zr interaction. However, the fact that the complex has a d⁰ configuration (considering the diene ligand as an enediyl) would seem to preclude any substantial back-bonding interaction, and this could lead to a weak agostic interaction and hence a relatively high C−H coupling constant. Indeed, a relatively high $J(^{13}C−H)$ value has been observed in another formally d⁰ complex believed to possess an agostic interaction.[79,80]

Thus, while the data at hand do not explicitly establish what sort of interaction is responsible for the small Zr−N−C angle, the overall situation is reminiscent of observations made by Popelier[78] on rotation of the methyl group in the CH₃TiCl₂ cation: "In going from the staggered to the eclipsed conformation, the C−H₃ bond becomes longer, the Ti−C−H₃ angle reduces to almost 90°, the ρ_b value is reduced, and the electron population of H₃ increases. These effects are collectively reminiscent of the formation of an agostic bond (potentially between Ti and H₃), although there is clearly no BCP present. So although both geometrical effects and AIM properties point in the direction of an α-agostic interaction, we do not find a bond expressing this interaction." A parallel situation was found for the agostic Ti(C₂H₅)Cl₃(dmpe) complex, wherein an extremely flat gradient path was observed, leading the authors to the expectation that bond critical points may not always be observed for agostic interactions.[34] The current results, together with the aforementioned observations, thus point to an interesting and important dichotomy concerning metal complexes with potential agostic interactions. It is clear that such a discrepancy between the ED results and the observed geometric distortions needs to be addressed in detail, for a proper understanding to be obtained for the bonding in these important types of complexes, and there is therefore a great need for further ED

and theoretical studies on a wide range complexes with agostic and/or π interactions.

Concluding Remarks

This high-resolution synchrotron X-ray diffraction study has allowed for the determination of an accurate crystal structure for the title zirconium complex as well as a complete ED analysis. We have shown that experimental determination of ED distributions and subsequent topological analysis are feasible even for second-row transition-metal-based organometallic compounds by minimizing absorption effects and using high-quality relativistic scattering factors.

The ED distribution and its topological analysis give new insight into the electronic structure of the title zirconium complex. Bond paths were observed between the zirconium center and the nitrogen atom, the diene, and dienyl ligands. Not surprisingly, the Zr−N interaction is strongest. Although only one bond path each is found linking the zirconium center with the diene/enediyl and dienyl ligands, electron density ellipticities indicate that π orbitals on the carbon atoms of these ligands interact with the metal center through polarization and hybridization effects, as also suggested by the spread-out lobes on the metal center and the electron density ellipticities in some of the unsaturated C−C bonds of the ligand. Comparing the diene/enediyl and dienyl bonding, the diene's C−C bonds have lower EDs and less negative Laplacians at their BCPs, but higher ellipticities than the dienyl C−C bonds, indicating stronger interactions of the metal center with the diene fragment. This is consistent with the diene's dianionic character and generally higher reactivity.[81]

The 4d atomic orbitals of Zr, derived from the modeled ED, exhibit unusual populations. The orbitals directed toward the ligands ($4d_{z^2}$ and $4d_{x^2-y^2}$) are not depopulated as could be expected from ligand field effects. The metal−ligand interactions are driven by σ-donation from both π ligands to the $4d_{z^2}$ orbital of zirconium, by σ-donation from N to the $4d_{x^2-y^2}$ orbital, and by π-donation from N to the $4d_{xz}$ orbital, in addition to a mean charge transfer of 2.16 e from Zr to the organic ligands, as derived by numerical integration of the ED over the topologically defined atomic basins.

Although the substantial distortion of the isopropyl group toward the zirconium center appears to indicate the presence of some sort of agostic interaction, the topological analysis of the ED in the region does not reveal any obvious indication that such an interaction exists. Thus, there is no bond path and corresponding BCP, and both structural and spectroscopic data also do not indicate obvious weakening of any bonds, which may be associated with agostic interactions. The ED analysis therefore does not provide an explanation for the small Zr−N−C16 angle and the proximity of the C−H bond and the metal atom. Additional studies will need to be undertaken to address this issue.[82]

In summary, these studies have provided the first experimental data concerning the electron density distribution in metal complexes with three (diene, dienyl, and amide) important types of ligands. They have revealed how the electron densities of these ligands respond to the presence of a zirconium atom and have thereby demonstrated that metal−ligand bonding interac-

(79) Thompson, M. E.; Baxter, S. M.; Bulls, A. R.; Burger, B. J.; Nolan, M. C.; Santarsiero, B. D.; Schaefer, W. P.; Bercaw, J. E. *J. Am. Chem. Soc.* **1987**, *109*, 203−219.

(80) It would be possible for both C−H and C−N interactions to occur with the Zr center, one serving to increase the C−H coupling constant and the other decreasing it.

(81) Basta, R.; Kulsomphob, V.; Ernst, R. D., unpublished results.
(82) Harvey, B. G.; Rheingold, A. L.; Ernst, R. D., work in progress.

tions may be present even in the absence of formal bond paths. It can be expected that systematic ED studies of key types of early through late organometallic compounds should lead to a much deeper understanding of σ, π, and agostic interactions in these compounds and to insight into key reactions such as oxidative additions and polymerizations.

Supporting Information Available: CIF file of the 16 K crystal structure. This material is available free of charge via the Internet at http://pubs.acs.org.

JA021133I